Journal of Materials Chemistry A

PAPER

View Article Online
View Journal | View Issue

Cite this: J. Mater. Chem. A, 2018, 6, 7741

Metal nanoparticle loading of gel-brush grafted polymer fibers in membranes for catalysis†

Yan Liu, [ab] Kaihuan Zhang, [b] Weiya Li, [c] Jinghong Ma *[a] and G. Julius Vancso *[b]

Received 5th February 2018
Accepted 21st March 2018

DOI: 10.1039/c8ta01231h

rsc.li/materials-a

We report on the preparation, characterization, and catalytic activity of microporous membranes featuring palladium (Pd) nanoparticles (NPs). The membranes consisted of polycaprolactone (PCL) microfibers featuring gel-brush layers of poly(hydroxyethyl methacrylate) (PHEMA). Pd nanoparticle loading was achieved by *in situ* reduction of Pd^{2+}, coordinated to carboxylate groups in the brush, in aqueous $Pd(NO_3)_2$ electrolytes by using $NaBH_4$. Gel-brushes were obtained *via* surface-initiated atom transfer radical polymerization (ATRP) polymerization. The membrane mats prior to functionalization were fabricated by electrospinning of PCL solutions. The PCL included mixtures of Br terminated PCL chains with a non-functional polymer. The electrospun fibers thus featured Br at their surface, which functioned as initiators, and allowed us to polymerize polymer gel-brushes at the fiber surface. The formation of Pd nanoparticles was evidenced by SEM and TEM. The membranes obtained had a large specific surface area and high porosity, which enabled high concentrations of metal nanoparticle loadings. The structure and morphology of the membranes were characterized by FTIR, SEM, TGA, and static contact angle measurements. The membranes obtained showed pronounced catalytic activity due to the presence of Pd NPs. As a proof-of-principle experiment we performed the catalytic reduction of 4-nitrophenol to 4-aminophenol in continuous flow-through catalysis.

1 Introduction

Porous membranes with a smart and functional surface have attracted broad attention because of their versatile applications in catalysis,[1,2] filtration,[3] and tissue engineering.[4] Porous membranes can also provide support for nanoparticle (NP) immobilization, which is very attractive for catalysis. The porous membrane geometry not only allows for flow-through reactions, but also facilitates the dispersion of particulate catalysts, and subsequently obtains products without further processing.[5] Moreover, high catalytic efficiency can be achieved due to high catalyst loading. The catalyst particles can be recovered,[6] which is usually cumbersome in the chemical process industry.

Among different membranes, microstructured reactors[7] have received distinguished attention in the chemical process industry in recent years.[8] Microreactors exhibit a remarkable catalytic efficiency because of their large available active surface. Such reactors are particularly interesting for chemical catalysis, especially for continuous flow-through reactions.

However, the size of most reported microreactors is still on the micrometer scale, which provides insufficient contact for the reagent solution and the catalyst.[9] Therefore, nanoscale porous substrates have been studied to improve this situation.[10] Porous electrospun membranes with high porosity, large surface area, and flexible channels can afford numerous functional sites which can be modified with polymer brushes. Moreover, functional polymer brushes when attached to electrospun membranes can be used to immobilize metal NPs.[11] By this method, nanoparticles can be distributed uniformly within the network.

Surface-initiated atom transfer radical polymerization (SI-ATRP)[12] was used to graft polymer brushes onto both flat and porous substrates.[13] In our previous work, we reported on the synthesis of poly(2-hydroxyethyl methacrylate) (PHEMA) polymer brush coatings coated onto the inner walls of glass microfluidic reactor channels, which can be applied to form, and *in situ* immobilize, silver and palladium nanoparticles, to be used as catalytic layers.[11] We also reported on the influence of the molecular architecture of gel-brush layers (such as the degree of cross-linking) on the size and size distribution of silver NPs.[13,14] Linear or cross-linked brushes were prepared. Cross-linking was achieved by the use of poly(ethylene glycol) dimethacrylate (PEGDMA).

[a]State Key Laboratory for Modification of Chemical Fibers and Polymer Materials, College of Materials Science and Engineering, Donghua University, 201620 Shanghai, P. R. China. E-mail: mjh68@dhu.edu.cn

[b]Materials Science and Technology of Polymers, MESA+ Institute of Nanotechnology, University of Twente, P.O. BOX 217, 7500 AE Enschede, The Netherlands. E-mail: g.j.vancso@utwente.nl

[c]Institut de Chimie de la Matière Condensée de Bordeaux (ICMCB-CNRS), 87 Avenue du Dr Albert Schweitzer, F-33608 Pessac Cedex, Pessac, France

† Electronic supplementary information (ESI) available. See DOI: 10.1039/c8ta01231h

To achieve high catalytic efficiency, the substrate should ideally feature a high specific surface area, and high catalyst loadings and porosity for the access of the reactants. For applications, the use of continuous flow-through (micro)reactors provides additional advantages. In this work we describe a catalytically active membrane, which can be used in continuous chemical reactions with high efficiency. The membrane consists of microporous, fibrous mats with fibers made of PCL. For the preparation of fibrous mats electrospinning of PCL solutions was employed. This allowed us to obtain fiber mats with a controlled thickness and fiber diameter displaying a very high surface area.[15] Following membrane fabrication, SI-ATRP was used to decorate the fiber surface within the membranes with gel brushes. This was enabled by using end-functionalized PCL for fiber spinning, which ensured the presence of abundant functional sites at the free surface of the fibers. Fig. 1 illustrates the process of obtaining the Pd NP loaded, microporous membrane. First, the Br–PCL–Br macroinitiator was synthesized and added to the precursor solution for electrospinning. PCL mats consisting of fibers that feature catalytically active Br sites at their free surface were thus obtained. Thus, the fibers in the porous PCL membrane embedded with initiators can be used as a substrate for grafting with PHEMA gel-brushes. Because of the high porosity of the membrane, gel-brushes would form across the membrane cross-section yielding a new layer on the surface of the fibers. This PHEMA gel-brush layer enhances the wettability of the membrane and supports permeability and diffusivity of reactants in aqueous systems. Due to the presence of primary hydroxyl groups in HEMA monomers, the gel-brush layers can be modified with succinic anhydride to yield COOH groups. Cross-linking to convert linear brush chains to a network was achieved by adding PEGMA as the cross-linker.[14] These cross-linked gel-brush layers were then employed as "nanoreactors" for the synthesis and immobilization of Pd nanoparticles. Pd^{2+} from aqueous palladium(II) nitrate ($Pd(NO_3)_2$) solutions when penetrating the membrane, associate with –COOH functionalities. *In situ* reduction of Pd^{2+} to yield Pd(0) and eventually Pd NPs was achieved by adding aqueous solutions of $NaBH_4$. We expect that Pd NPs in the gel-brush structure will act as the catalyst. In order to prove the catalytic activity, the "standard" catalytic reduction reaction of 4-nitrophenol (4-NP) to 4-aminophenol (4-AP) was employed using Pd NP loaded membranes in flow-through reactions. The results as shown by this study clearly demonstrated a high catalytic enhancement.

2 Experiment

2.1 Materials

Polycaprolactone (PCL, average $M_n \sim 80\,000$ g mol^{-1}), polycaprolactone (HO–PCL–OH, average $M_n \sim 10\,000$ g mol^{-1}), 2-hydroxyethyl methacrylate (HEMA, 97%), poly(ethylene glycol) dimethacrylate (PEGDMA, average $M_n \sim 550$ g mol^{-1}), succinic anhydride, α-bromoisobutyryl bromide (BIBB, 98%), triethylamine (TEA), dichloromethane (DCM), copper(I) bromide (CuBr), copper(II) bromide ($CuBr_2$), 2,2′-bipyridine (bipy), sodium borohydride ($NaBH_4$), palladium(II) nitrate dihydrate ($Pd(NO_3)_2 \cdot 2H_2O$), 4-nitrophenol (4-NP), 4-aminophenol (4-AP), methanol, phosphate buffered saline, and sodium hydroxide were supplied by Sigma-Aldrich. With the exception of HEMA and CuBr all reactants were used as received. 2-Hydroxyethyl methacrylate was purified by distillation under reduced pressure. Copper(I) bromide was stirred in excess acetic acid, filtered, and dried using a vacuum oven at room temperature

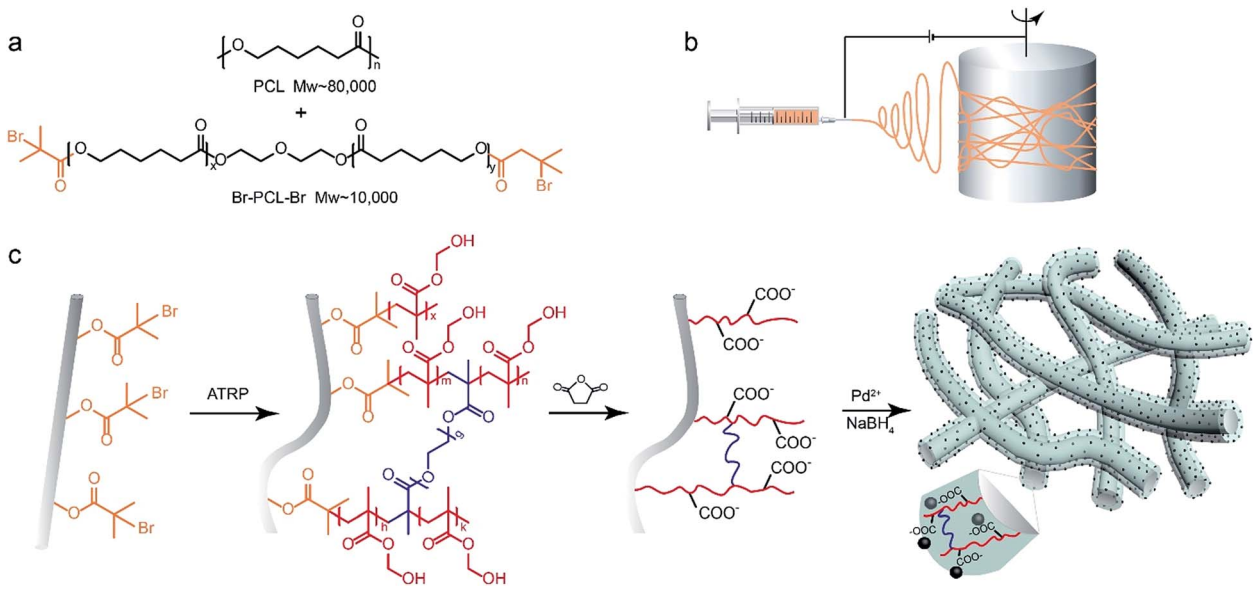

Fig. 1 Preparation steps of catalytically active, fibrous membranes. (a) PCL and end-functional Br–PCL–Br used in solutions for electrospinning to yield microporous, fibrous mats as the membrane support. (b) Electrospinning of PCL membranes featuring Br at their surface used as ATRP initiators. (c) Preparation steps to obtain Pd NP loaded gel-brush layers; from left to right: PCL fibers in the membrane with the SI-ATRP initiator; one step gel-brush SI ATRP to yield cross-linked HEMA gel-brushes; acidification with succinic anhydride; *in situ* reduction to yield Pd NPs immobilized in the gel-brush layer.

overnight. Water was purified with a Milli-Q Advantage A10 purification system (Millipore, Billerica, MA, U.S.A.).

2.2 Synthesis of the Br–PCL–Br macroinitiator

First, the HO–PCL–OH (5 g) was dissolved in anhydrous dichloromethane (50 mL) with TEA (500 μL) under argon protection and cooled in an ice-water bath. An excess of BIBB (430 μL) was then added dropwise to the solution. The mixture was stirred for 24 hours to achieve completion of the reaction. The final product was precipitated with an excess of methanol, followed by filtration, and subjected to three precipitation cycles. The macroinitiator was stored under nitrogen prior to electrospinning.

2.3 Preparation of electrospun porous membranes decorated with initiators

The porous membranes decorated with initiators were fabricated by electrospinning. The weight ratio of the PCL substrate and Br–PCL–Br macroinitiator was 100 : 20. The concentration of the PCL substrate was 0.1 g mL^{-1} and the final content of Br in the polymer was 0.27 wt%. The polymer precursor solution was stirred overnight prior to electrospinning. The custom-built electrospinning set-up used consisted of a high voltage power supply and a rotating drum (Fig. 1b). The voltage of the transverse electric field between the spinneret tip and the rotator was 11.5 kV. The injection rate was controlled by using a pump (KDS 100 Legacy Syringe Pump, KD Scientific) and was set to 1 mL min^{-1}. The distance between the spinneret tip (with a diameter 0.9 mm) and the rotating drum was 13 cm and the rotation speed of the drum (diameter 15 cm) was set to 400 rpm. After typically 4–5 h of spinning at room temperature, the process was stopped, and porous electrospun membranes decorated with Br initiators were obtained. The membranes fabricated were removed from the drum and transferred into an oven at 40 °C to evaporate the solvent. Typical (average) fiber diameters were in the range of 400–450 nm (Fig. S1a, ESI†).

2.4 Preparation of catalytically active membranes

Porous electrospun membranes featuring Br terminated initiators were grafted with PHEMA gel-brushes by SI-ATRP. During polymerization first purified monomer HEMA (4.8 g) and bipyridine (0.29 g) were added to water (20 mL). The solution was degassed with argon for 30 min. The solution was subsequently transferred, using a degassed syringe, into a glass flask flushed with argon containing CuBr (53 mg) and $CuBr_2$ (8 mg). The final ratio of the reactants was as follows: HEMA : CuBr : $CuBr_2$: bipy = 100 : 1 : 0.1 : 5. This mixture included 2 mol% poly(ethylene glycol) dimethacrylate (PEGDMA) as the cross-linker.

The mixture was stirred at ambient temperature for 30 min to form a burgundy-colored complex. Subsequently, the burgundy-colored solution was transferred, using a degassed syringe, into an argon-purged flask containing the PCL initiator functionalized porous electrospun membrane to perform SI-ATRP. The typical polymerization time was 4 hours at room temperature. The resulting brush-decorated membranes were extracted from the solution and washed three times with water and ethanol. The membrane then was derivatized with succinic anhydride (30 mg mL^{-1} in dry DMSO solution) in order to introduce carboxylic acid moieties along the polymer backbones. PEGMA was used as the cross-linker.

In order to prepare gel-brush/Pd NPs membranes, these membranes were immersed overnight in an aqueous $Pd(NO_3)_2$ solution (5.33 mg mL^{-1}). Then the membranes were immersed for 10 seconds into a solution of $NaBH_4$ (0.38 mg mL^{-1}) in order to *in situ* reduce the Pd(II) ions in the brush structure to yield Pd(0) NPs.

2.5 Flow-through catalysis of reducing 4-NP to 4-AP

The setup for performing flow-through reactions consisted of a filter holder (Swinnex Filter Holder, 13 mm, Sigma) and a syringe pump. The catalytically active membrane was put into the filter containing a cellulose membrane as the support. To perform the flow-through reactions, an aqueous solution of 4-NP (0.014 mg mL^{-1}) with $NaBH_4$ (0.38 mg mL^{-1}) was forced through the membrane. Reagent solutions were injected by using a syringe pump (PHD Ultra, Harvard Apparatus) in these experiments. The products were collected and analyzed by UV-Vis spectroscopy to determine the concentration of the reaction product, and the catalytic efficiency. All experiments were carried out at room temperature.

2.6 Characterization methods

^1H NMR spectra were collected on a Bruker Avance III spectrometer operated at 400 MHz. The samples were dissolved in $CDCl_3$ and spectra were recorded at room temperature. Chemical shifts (δ) were expressed with respect to the $CDCl_3$ signals. The morphology of gel-brush membranes and catalytically active membranes with Pd NPs was recorded by SEM (Field Emission JSM-633OF, JEOL Benelux) and TEM (CM300, FEI/Philips). FTIR spectra (with a spectral resolution of 4 cm^{-1}, 256 scans) were obtained using an FTIR spectrometer (Nicolet 6700, Thermo Fisher). The thickness of the gel-brush layers on the fibers was about 80 nm estimated by using film thickness values obtained on planar substrates when measured with ellipsometry.[13] In addition, layer thickness values were also estimated by measuring fiber diameters using SEM images (Fig. 3a and b). As the fibers show a broad distribution, only average values (600–650 nm, Fig. S1b, ESI†) could be obtained. XPS was performed on a PHI Quantera SXM-XPS system. Fiber mat wettability was estimated by measuring static contact angle values (OCA20, Dataphysics, Germany). TGA (TGA7, Waltham, MA, USA) was used to characterize the relative compositions of the membranes decorated with initiators, membranes decorated with PHEMA gel-brushes, and catalytically active membranes with Pd NPs. The concentrations of reactants in the aqueous solutions and solutions of the reaction products were monitored by a flow-through reaction using UV-Vis spectroscopy (LAMBDA 850, Perkin Elmer).

3 Results and discussion

3.1 Synthesis of the Br–PCL–Br macroinitiator

The Br–PCL–Br macroinitiator was synthesized by a substitution reaction, replacing terminal –OH groups with –Br. In order

to verify the formation of the initiator, both the HO–PCL–OH reactant and the product were characterized by ^{1}H NMR. The results are shown in Fig. S2 in the ESI.† The ^{1}H NMR spectra proved the formation of end groups with active Br for ATRP polymerization (yield: 95.9%). The samples were dissolved in $CDCl_3$ and the spectra were recorded at room temperature. Chemical shifts (δ) were expressed with respect to the $CDCl_3$ signals. The ^{1}H NMR spectrum of HO–PCL–OH presents the characteristic signals of methylene (–CH_2–) groups in PCL (δ = 1.31, 1.58, 2.24, and 3.99 ppm). After using BIBB to exchange the –OH end groups, a new signal at 1.86 ppm appeared in the spectra due to the presence of methyl (–CH_3) groups in the structure of BIBB[16] as shown in Fig. S2.† In addition, the proportion of –CH_3 in the Br–PCL–Br initiator is nearly 7% which means that nearly all end groups (–OH) were substituted by groups terminated by Br.

3.2 FTIR of membranes

PHEMA grafted PCL membranes were prepared by SI-ATRP. The PCL membrane including macroinitiators, PCL–PHEMA gel-brush membrane, and PCL–PHEMA gel-brush membrane treated with a buffer solution (pH = 10) were characterized by FTIR and the results are shown in Fig. 2. According to the spectrum of a pure PCL membrane without modification, strong carbonyl stretching bands around 1700 cm^{-1} characteristic of PCL can clearly be seen.[17] A new peak at 647 cm^{-1} corresponding to C–Br appears for the PCL membrane including macroinitiators. The spectrum for the PCL–PHEMA gel-brush not only presented a characteristic C=O stretching band at 1700 cm^{-1}, but also displayed a broad shoulder at 3400 cm^{-1}. This is assigned to the presence of –OH groups in the hydroxyethyl methacrylate monomer units. After acidification with succinic anhydride and treatment with a buffer solution, the relative intensity of the peak corresponding to the C=O stretching increased and a peak with a relatively low absorbance appeared at 1580 cm^{-1} indicating the stretching of the COO– functionalities. All FTIR results indicate that the functional gel-brushes were grafted onto the surface of the electrospun nanofibers.

3.3 Wettability of membranes

As can be seen from Fig. S3a (ESI†), for PCL electrospun porous membranes, the value of the contact angle is 131°, which indicates that this membrane was hydrophobic at room temperature.[18] SI-ATRP of PHEMA brushes rendered the fiber surface hydrophilic (Fig. S3b†). The value of the contact angle of the PCL–PHEMA gel-brush porous membrane changed to 0° due to the presence of hydrophilic OH end groups of PHEMA chains and the capillary effect of the microporous structure.[19] Enhanced hydrophilicity of the PHEMA gel-brush layer supports the loading of catalyst NPs and will benefit the permeability of aqueous reagent solutions for catalysis.

3.4 Surface morphology of the membranes

The surface morphology of the PCL membrane with embedded macroinitiators, the PCL–PHEMA gel-brush membrane, and the PCL–PHEMA/Pd NP catalytically active membrane was characterized by SEM. Fig. 3a–c show the morphology of different membranes. The surface of the PCL electrospun nanofibers fabricated by electrospinning was smooth as exhibited in Fig. 3a. After gel-brush grafting, the diameter of the nanofibers obviously increases. It is interesting to mention that a pronounced curvature and fiber bending appears following grafting (Fig. 3b). We believe that this is in part related to stresses along the fiber axial directions that originate from brush swelling. After the reduction of Pd(II) ions in the gel-brush

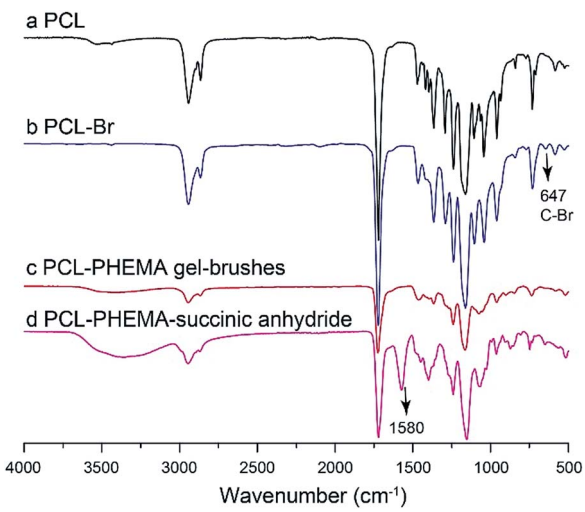

Fig. 2 FTIR of (a) pure PCL membranes, (b) PCL membranes including macroinitiators, (c) PCL–PHEMA gel-brush grafted membranes prepared by ATRP, and (d) PCL–PHEMA gel-brush grafted membranes acidified with succinic anhydride and then treated with buffer (pH = 10).

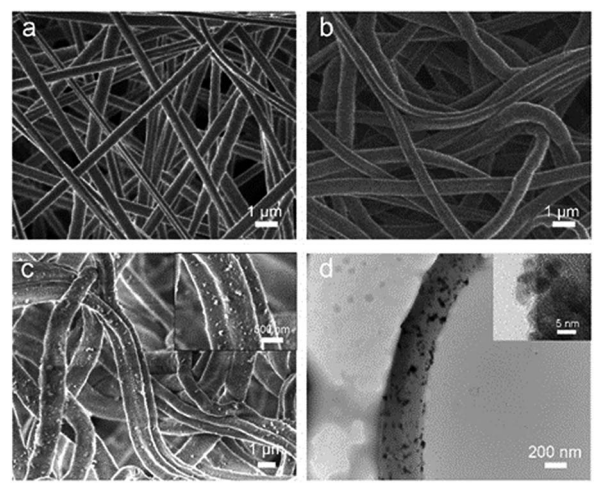

Fig. 3 Surface morphology of the membranes. (a) PCL membrane with macroinitiators. (b) Membrane with fibers decorated with PCL–PHEMA gel-brushes. (c) PCL–PHEMA/Pd NP containing catalytic membrane (inset in the top right corner: enlarged magnification showing the morphology of one fiber). (d) HR-TEM image of Pd NPs obtained by *in situ* reduction in the gel-brush layer.

to Pd(0), metal nanoparticles can be found homogeneously distributed on the surface of the nanofibers (Fig. 3c). We note that although we do not have direct evidence supporting the presence of NPs in the gel-brush interior, this can be assumed based on our earlier results.[15] EDX spectra also show the presence of Pd (Fig. S4 in the ESI†). XPS spectra show double peaks with binding energies at 335.1 eV and 340.5 eV, corresponding to $Pd3d_{5/2}$ and $Pd3d_{3/2}$, respectively (Fig. S5 in the ESI†). Compared to the standard spectra of Pd(0), the binding energies are in good agreement with the expected values for Pd(0).[20,21] The presence of a microporous membrane morphology can be clearly seen from Fig. 3c, which will allow reactants to flow through the catalytically active membrane.

In addition, nanofibers in membranes not only provide channels in the membrane-perpendicular direction but also contribute to diffusive flow along gel-brush grafted nanofibers. These flow patterns provide sufficient contact between reactant-containing solutions and nanoparticle catalysts in the membrane, thus supporting the anticipated high catalytic efficiency of the membrane.

In order to verify the presence of metal nanoparticles, catalytically active nanofibers were imaged by TEM. The high resolution TEM image of the nanoparticles *in situ* formed in the gel-brush layer is shown in Fig. 3d. The nanoparticles were distributed densely and evenly on the surface of the nanofibers. The high magnification TEM image indicates that these nanoparticles include single crystals with several [111] facets.[22,23] The measured interplanar spacing for the lattice fringes is 0.22 nm, corresponding to metallic Pd [111].[24] The diameter of individual Pd nanoparticles was in the range of 3–5 nm.

3.5 Thermal gravimetric analysis (TGA)

Thermal gravimetric analysis (TGA) of PCL, PCL–PHEMA, and PCL–PHEMA/Pd NP electrospun porous membranes was performed in an N_2 atmosphere. The results obtained are shown in Fig. 4. For the pure PCL membrane, substantial weight loss was found at 440 °C and the residual mass approached 0% indicating full polymer loss. For the PCL–PHEMA gel-brush membrane, the weight loss took place at two different temperatures. The two peaks shown in the derivative thermal gravimetric (DTG) curve were located at 310 °C for PHEMA[25] and 440 °C for PCL, which supports the successful formation of the PHEMA gel-brush on the surface of the nanofibers with a decomposition temperature around 310 °C. After loading with Pd NPs, the membrane was washed and then analyzed also by TGA. From the residual mass a Pd loading of 54.9 w/w% was obtained. This high weight percentage can be rationalized by the much higher density of the metal than polymers.

3.6 Catalytic efficiency of membranes with Pd NPs

The catalytic performance of the membranes was demonstrated, as mentioned, by performing the reduction of 4-nitrophenol (4-NP) to 4-aminophenol (4-AP) in water at room temperature. The microporous structure of the membranes facilitated performing the reaction in flow-through geometry.

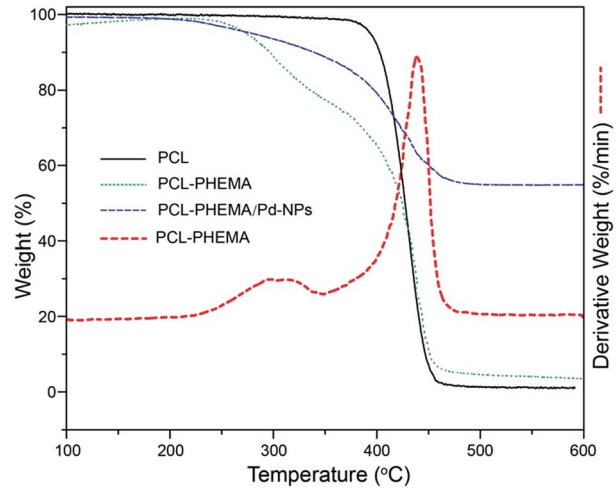

Fig. 4 TGA results of PCL, PCL–PHEMA gel-brush, and PCL–PHEMA/Pd NP porous membranes. DTG result of the PCL–PHEMA gel-brush electrospun porous membrane.

The setup and the filter used in these experiments systems with a catalytic membrane are illustrated in Fig. 5d.

The kinetics of this reaction can be described by the Langmuir–Hinshelwood (LH) model.[26,27] Before the reaction, the reactants are adsorbed on the surface of nanoparticles, and the adsorption is fast according to the equilibrium process *e.g.* described by the Langmuir isotherm. Finally, the reaction product detaches from the surface of the catalytic nanoparticles.[28,29] Moreover, when an excess of $NaBH_4$ is used, this reaction is usually regarded as a first-order reaction, and the kinetics can be described using the following equation with UV absorbance of the product (A_t) and the reactant (A_0):

$$\ln(A_t/A_0) = \ln(C_t/C_0) = -kt \text{ (see ref. 30)}$$

where C_t represents the concentration of the reaction product 4-AP, C_0 is the concentration of 4-NP, and t is the residence time.

According to the LH model,[31] Pd NPs display better catalytic activity than other metal nanoparticles (AgNPs or AuNPs) due to the easier adsorption of hydrogen on the Pd surface. Thus Pd NPs were selected as the loading of PCL–PHEMA gel-brush membranes for the purpose of demonstrating the catalytic activity.

The value of the pseudo-first-order rate constant was proportional to the concentration of $NaBH_4$ and affected by the geometric features of the nanoparticles.[11,32,33] The concentration of $NaBH_4$ in all experiments was held constant and the membrane reactors were prepared and kept under the same conditions.

The reduction process from 4-NP to 4-AP actually involves two steps.[34] First, 4-NP combines rapidly with the OH^- hydrolyzed by sodium borohydride to convert to 4-nitrophenolate ions (4-NPI). Then, 4-NPI is reduced by the Pd NPs in the porous membrane to 4-AP.

The absorbance peak of 4-NP should be at 320 nm, while a shift to 400 nm due to the formation of 4-NPI is expected.[35] Fig. 5b shows the UV-Vis absorption spectra of the solution

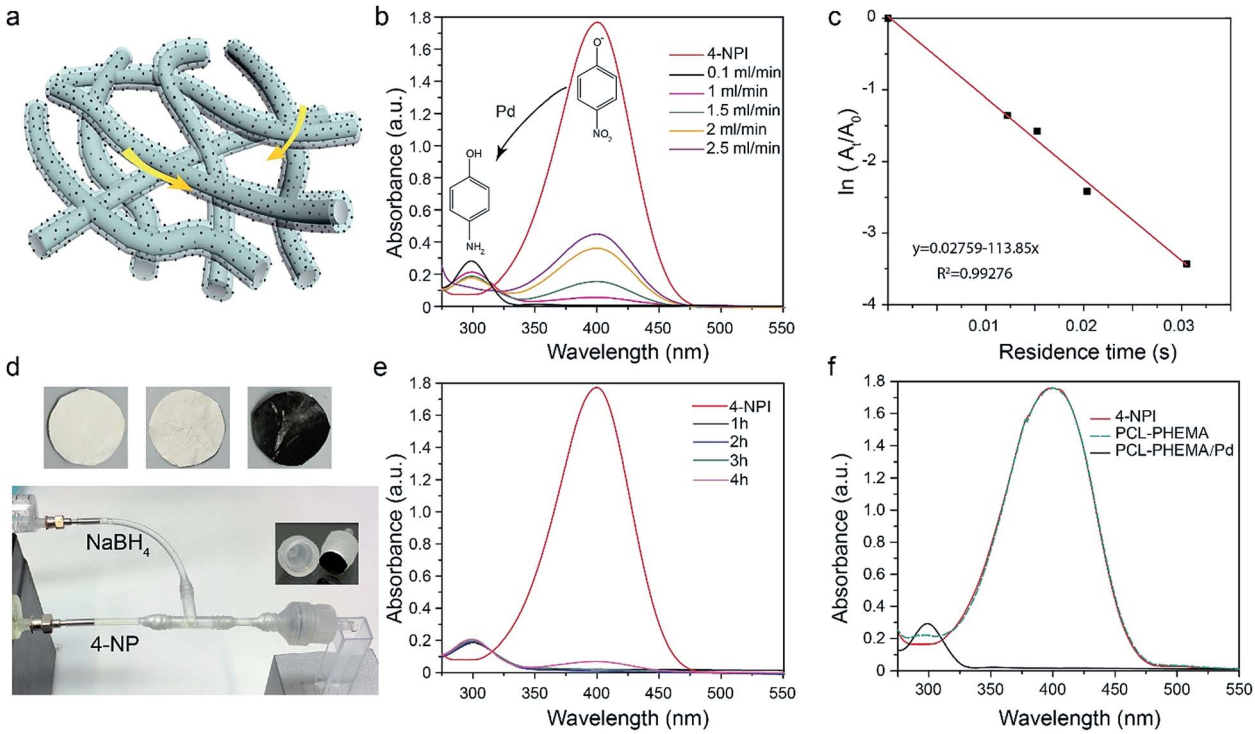

Fig. 5 Efficiency of the catalytically active electrospun mats. (a) PCL–PHEMA gel-brush/Pd NP membrane (gel-brush layer marked with blue color). The arrows show two routes of how the reagent solution flows through the membrane: one is through the nanopores and the other one is along the gel-brush layer. (b) UV-Vis absorption spectra of the 0.1 mM 4-NP, 10 mM $NaBH_4$ solution passing through the porous membrane catalyzed by Pd NPs at different flow rates. (c) Plot of $\ln(A_t/A_0)$ against the reaction time. (d) Photographs of the representative membranes and filter holder (membrane diameter = 1.3 cm). Membranes from left to right: the membrane with the SI-ATRP initiator; PHEMA gel-brush decorated membrane; catalytically active membrane. (e) Relationship between the conversion and duration time of the catalytic reaction at 0.1 mL min^{-1} flow rate. (f) UV-Vis absorption spectra of the 0.1 mM 4-NP, 10 mM $NaBH_4$ solution flowed through the PCL membrane without modification and PCL–PHEMA membrane without nanoparticles.

passed through the PCL–PHEMA/Pd NPs membrane. The reaction time was varied by changing the flow rates from 0.1 to 2.5 mL min^{-1}. At a very low flow rate corresponding to a long residence time, the absorption peak of 4-NP essentially disappears which means that the conversion is close to quantitative (the catalytic efficiency is more than 99.9% at 0.1 mL min^{-1}). With the increase of the flow rate, the absorption peak increases, which means that the conversion of 4-NP is decreased due to the shortened residence time of the reagent solution in the PCL–PHEMA/Pd NPs membrane. The catalytic efficiencies of catalytically active membranes at flow rates from 1 to 2.5 mL min^{-1} are 97%, 91%, 79%, and 74%, respectively. The product flows out of the membrane continuously, ensuring continuous operation of the catalytic NPs. Finally, we also note that this flow-through reaction minimized the possibility of side reactions due to short residence times.[10]

Fig. 5c shows the observed relationship between $\ln(A_t/A_0)$ and the residence time of solutions in the PCL–PHEMA/Pd NPs gel-brush membrane during 4-NP flow through the membrane. The residence time could be estimated from the total volume of the solution flowing through the membrane divided by the corresponding flow rate. This was estimated by first weighting the membranes without water, and then determining the mass with water. For the membrane species investigated in the catalytic reaction, we found that it could absorb 0.5 mg of water. (We note that due to the small amounts of water this value can include statistical errors in the range of 5–10%. The mass of water that can be absorbed by a given membrane was determined from the average weight of 10 membranes.) For the flow through reduction experiment, the lowest flow rate used was 0.1 mL min^{-1}. As the electrospun membrane is very thin (the thickness of the catalytically active membranes is 20 μm), the residence time in the membrane is quite short, only around 0.03 s at 1 mL min^{-1}. The kinetic analysis of the reduction of 4-NP was carried out by using an excess of $NaBH_4$, and the first-order rate constant was calculated by linear fitting. After performing a simple linear regression, the value of the slope shown in Fig. 5c is −114 (s^{-1}), yielding a rate constant value of 114 s^{-1}. When we compare this result with those of previously published research studies (first-order rate constant 0.034 s^{-1}, 0.24 min^{-1}, and 1 min^{-1}),[11,36,37] it can be seen that the catalytic activity of the porous catalytically active membrane has been enhanced significantly.

One reason for the high catalytic efficiency should be related to the high loading of Pd NPs, related to the high surface area of the catalytic membrane. Another important point is that the porous membrane provides a "tortuous route" for the reactant solution which enhances better access to the catalyst NPs.

In order to test the stability of the catalytically active membrane, long catalytic runs were performed. As shown in Fig. 5e, the UV-Vis absorption spectra of reaction products following membrane permeation were collected after 1 h and 4 h. In these experiments, the aqueous reactant solution was injected continuously through the membrane (0.1 mL min^{-1}), and 4-AP was produced with a high conversion rate. The reduction of 4-NP is more than 99% in 60 min and decreases to 96% after 4 hours.

There are two possible reasons for the decline of conversion values observed. One is that the amount of the reducing agent in the reagent solution decreases with time due to continuous $NaBH_4$ degradation.[38] The other one is that the by-products may block the catalytic sites of the nanoparticles.[39]

Additionally, Pd NPs may get washed out over longer periods of reactions, and moved to the solution of the reaction product. We checked the permeated solutions by UV-Vis spectroscopy for the presence of Pd nanoparticles (Fig. S6, ESI†). The spectra showed no measurable presence of Pd NPs. The reagent solution was also flowed through the PCL membrane without modification and PCL–PHEMA gel-brush membrane without nanoparticles as blank reference experiments. The results obtained are shown in Fig. 5f. It is evident that no reaction occurred in these two membranes without nanoparticles.

4 Conclusions

Catalytic membranes featuring PHEMA gel-brushes were obtained *via* SI-ATRP with Pd NP loadings. NPs were formed by the reduction of Pd^{2+} in aqueous $Pd(NO_3)_2$ solutions. Electrospun PCL gel-brush supporting fibers as substrates were prepared. The PCL encompassed mixtures of Br terminated polymer chains with a non-functionalized polymer, which allowed us to grow PHEMA polymer gel-brushes on the surface of nanofibers in the electrospun, nanoporous membranes. The successful synthesis of the ATRP active macroinitiator was checked by ^1H NMR. The PCL–PHEMA gel-brush membranes were characterized by FTIR and the results prove that the membranes were successfully modified with PHEMA gel-brushes. This finding was also supported by the increased wettability of the membranes. The morphology of the PCL–PHEMA gel-brush membrane was characterized by SEM and the results show nanofibers with an average diameter in the range of 600–650 nm. Pd NPs with a diameter in the range between 3 and 5 nm were obtained within the brush-decorated microfibrous membrane mats by *in situ* reducing metallic cations from electrolytes using $NaBH_4$ as the reducing agent. NP formation and distribution along the fibers were visualized by TEM. The thus obtained catalytically active membranes were used in continuous flow-through catalysis of reducing 4-nitrophenol to 4-aminophenol. The UV-Vis spectra of the reagent and the product solution indicated high efficiency of the catalytic membranes. The results confirmed that this membrane has a high catalytic activity and has potential for application in the chemical industry.

Conflicts of interest

There are no conflicts to declare.

Acknowledgements

We thank the MESA+ Institute of Nanotechnology of the University of Twente for financial support. K. Z. thanks the Netherlands Organization for Scientific Research (NWO 728.011.205) for funding, and Y. L. expresses her appreciation to the Chinese Scholarship Council for a graduate studies scholarship. The authors thank Mr Clemens Padberg for obtaining the SEM images.

References

1 S. Ma, J. Liu, Q. Ye, D. Wang, Y. Liang and F. Zhou, *J. Mater. Chem. A*, 2014, **2**, 8804–8814.
2 F. Costantini, W. P. Bula, R. Salvio, J. Huskens, H. J. Gardeniers, D. N. Reinhoudt and W. Verboom, *J. Am. Chem. Soc.*, 2009, **131**, 1650–1651.
3 J. Wu, N. Wang, H. Zhang, L. Wang, H. Dong, Y. Zhao and L. Jiang, *J. Mater. Chem. A*, 2013, **1**, 4642–4646.
4 M. Vallet-Regí, F. Balas and D. Arcos, *Angew. Chem.*, 2007, **46**, 7548–7558.
5 D. M. Dotzauer, J. Dai, L. Sun and M. L. Bruening, *Nano Lett.*, 2006, **6**, 2268–2272.
6 H. Hu, J. H. Xin and H. Hu, *J. Mater. Chem. A*, 2014, **2**, 11319–11333.
7 P. Watts and C. Wiles, *Chem. Commun.*, 2007, 443–467.
8 K. Jähnisch, V. Hessel, H. Löwe and M. Baerns, *Angew. Chem.*, 2004, **43**, 406–446.
9 L. Li, S. Peng, J. K. Y. Lee, D. Ji, M. Srinivasan and S. Ramakrishna, *Nano Energy*, 2017, **39**, 111–139.
10 J. Liu, S. Ma, Q. Wei, L. Jia, B. Yu, D. Wang and F. Zhou, *Nanoscale*, 2013, **5**, 11894–11901.
11 F. Costantini, E. M. Benetti, R. M. Tiggelaar, H. J. Gardeniers, D. N. Reinhoudt, J. Huskens, G. J. Vancso and W. Verboom, *Chem.–Eur. J.*, 2010, **16**, 12406–12411.
12 R. Barbey, L. Lavanant, D. Paripovic, N. Schüwer, C. Sugnaux, S. Tugulu and H.-A. Klok, *Chem. Rev.*, 2009, **109**, 5437–5527.
13 X. Sui, S. Zapotoczny, E. M. Benetti, M. Memesa, M. A. Hempenius and G. J. Vancso, *Polym. Chem.*, 2011, **2**, 879–884.
14 E. M. Benetti, X. Sui, S. Zapotoczny and G. J. Vancso, *Adv. Funct. Mater.*, 2010, **20**, 939–944.
15 X. Zong, K. Kim, D. Fang, S. Ran, B. S. Hsiao and B. Chu, *Polymer*, 2002, **43**, 4403–4412.
16 T. Du, B. Li, X. Wang, B. Yu, X. Pei, W. T. Huck and F. Zhou, *Angew. Chem.*, 2016, **55**, 4260–4264.
17 T. Elzein, M. Nasser-Eddine, C. Delaite, S. Bistac and P. Dumas, *J. Colloid Interface Sci.*, 2004, **273**, 381–387.
18 M. Ma, Y. Mao, M. Gupta, K. K. Gleason and G. C. Rutledge, *Macromolecules*, 2005, **38**, 9742–9748.
19 S. Kaur, Z. Ma, R. Gopal, G. Singh, S. Ramakrishna and T. Matsuura, *Langmuir*, 2007, **23**, 13085–13092.

20 S. Yang, J. Dong, Z. Yao, C. Shen, X. Shi, Y. Tian, S. Lin and X. Zhang, *Sci. Rep.*, 2014, **4**, 4501.
21 S. Shanmugam, B. Viswanathan and T. K. Varadarajan, *Nanoscale Res. Lett.*, 2007, **2**, 175–183.
22 P. Zhang, Y. Gong, H. Li, Z. Chen and Y. Wang, *Nat. Commun.*, 2013, **4**, 1593.
23 T. Teranishi and M. Miyake, *Chem. Mater.*, 1998, **10**, 594–600.
24 Z. R. Dai, J. P. Bradley, D. J. Joswiak, D. E. Brownlee, H. G. M. Hill and M. J. Genge, *Nature*, 2002, **418**, 157–159.
25 S.-L. Huang, W.-K. Chin and W. P. Yang, *Polymer*, 2005, **46**, 1865–1877.
26 S. Wunder, Y. Lu, M. Albrecht and M. Ballauff, *ACS Catal.*, 2011, **1**, 908–916.
27 S. Wunder, F. Polzer, Y. Lu, Y. Mei and M. Ballauff, *J. Phys. Chem. C*, 2010, **114**, 8814–8820.
28 Y. Mei, G. Sharma, Y. Lu, M. Ballauff, M. Drechsler, T. Irrgang and R. Kempe, *Langmuir*, 2005, **21**, 12229–12234.
29 Y. Kang and T. A. Taton, *Macromolecules*, 2005, **38**, 6115–6121.
30 Y.-N. Chen and H. Wang, *J. Colloid Interface Sci.*, 2015, **454**, 14–19.
31 D. Huang, G. Yang, X. Feng, X. Lai and P. Zhao, *New J. Chem.*, 2015, **39**, 4685–4694.
32 S. Cao, F. F. Tao, Y. Tang, Y. Li and J. Yu, *Chem. Soc. Rev.*, 2016, **45**, 4747–4765.
33 U. Hartfelder, C. Kartusch, M. Makosch, M. Rovezzi, J. Sa and J. A. van Bokhoven, *Catal. Sci. Technol.*, 2013, **3**, 454–461.
34 J. Wu, W. Liu, X. Xiang, K. Sun, F. Liu, C. Cai, S. Han, Y. Xie, S. Li and X. Zu, *Carbon*, 2017, **117**, 192–200.
35 W. Lu, R. Ning, X. Qin, Y. Zhang, G. Chang, S. Liu, Y. Luo and X. Sun, *J. Hazard. Mater.*, 2011, **197**, 320–326.
36 A. Gangula, R. Podila, M. Ramakrishna, L. Karanam, C. Janardhana and A. M. Rao, *Langmuir*, 2011, **27**, 15268–15274.
37 J. Min, F. Wang, Y. Cai, S. Liang, Z. Zhang and X. Jiang, *Chem. Commun.*, 2015, **51**, 761–764.
38 L. Ouyang, D. M. Dotzauer, S. R. Hogg, J. Macanás, J.-F. Lahitte and M. L. Bruening, *Catal. Today*, 2010, **156**, 100–106.
39 T. Vincent and E. Guibal, *Langmuir*, 2003, **19**, 8475–8483.